PHYSICAL REVIEW D VOLUME 24, NUMBER 5 1 SEPTEMBER 1981

Baryon-antibaryon threshold and ω-baryonium mixing

R. V. Gavai
Tata Institute of Fundamental Research, Homi Bhabha Road, Bombay 400005, India
(Received 27 February 1980)

It is shown that in any dual-topological-unitarization model of ω-baryonium ($\mathfrak{B}$) mixing at the cylinder level, in which the production of baryon-antibaryon ($b\bar{b}$) pairs can take place only above a certain threshold energy, the phenomenologically relevant ω and $\mathfrak{B}$ trajectories do not mix below $b\bar{b}$ threshold. However, their couplings to external particles do get modified. The ω-$\mathfrak{B}$ mixing angle $\theta_{\omega\text{-}\mathfrak{B}}$, which characterizes these coupling modification effects below $b\bar{b}$ threshold at $t = 0$, is estimated in some models. These estimates are found to agree reasonably well with the existing phenomenological bound on $\theta_{\omega\text{-}\mathfrak{B}}$.

I. INTRODUCTION

It is well known that in most of the dual-topological-unitarization (DTU) models of the Pomeron some mechanism such as mixing with lower-lying trajectories has to be invoked to boost up the cylinder-depressed ω trajectory.[1] Thus mixing with ϕ (Ref. 2) and/or baryonium[3-5] ($\mathfrak{B}$) has been used in the literature to achieve a phenomenologically acceptable ω intercept. Amongst the models which invoke $\mathfrak{B}$ mixing, there is a large disagreement in the predicted amount of ω-$\mathfrak{B}$ mixing below the baryon-antibaryon ($b\bar{b}$) production threshold. Thus the predictions of Refs. 3 and 4 are in strong disagreement with a phenomenological bound on the ω-$\mathfrak{B}$ mixing parameter $\sin\theta_{\omega\text{-}\mathfrak{B}}$, obtained by Gavai and Roy[6] (e.g., Ref. 3 predicts $\sin\theta_{\omega\text{-}\mathfrak{B}} = 0.76$, while the bound of Ref. 6 is $|\sin\theta_{\omega\text{-}\mathfrak{B}}| < 0.26$),[7] while the predictions of Ref. 5 do obey the bound, provided the input parameters are constrained in a reasonable way.

Of course, it is true that the models of Refs. 3 and 4 are based on a different realization of DTU, namely the one-dimensional approximation scheme of Kwiecinski and Sakai,[8] than that of Ref. 5, which is a simple extension of the Chew-Rosenzweig[2] (CR) scheme. But still, in view of the fact that both Refs. 4 and 5 consider ω-ϕ-$\mathfrak{B}$ mixing schemes only, the difference in their predictions of $\theta_{\omega\text{-}\mathfrak{B}}$ appears quite puzzling. Attempting to resolve this puzzle, one notes that $b\bar{b}$ threshold effects were ignored for simplicity in the work of Ref. 5, which, however, were included in Refs. 3 and 4. On the other hand, detailed dynamical assumptions were made in Refs. 3 and 4 in order to formulate the bootstrap equations and these may be inconsistent with data. We have, therefore, chosen to investigate a general DTU model of ω-$\mathfrak{B}$ mixing in the presence of $b\bar{b}$ threshold effects for an answer to the above mentioned puzzle. We find, as we show in this paper, that in any such model the phenomenologically relevant ω and $\mathfrak{B}$ trajectories do not mix below the $b\bar{b}$ threshold. However, in general, their couplings to external particles do get modified. Therefore, a nonzero $\theta_{\omega\text{-}\mathfrak{B}}$, corresponding to the phenomenological quantity on which Ref. 6 obtained a bound, is possible.

Turning to the one-dimensional models, we find that due to their predictive power, an explicit calculation of $\theta_{\omega\text{-}\mathfrak{B}}$ is possible and in models with essentially the same assumptions as Refs. 3 and 4 the estimates of $\theta_{\omega\text{-}\mathfrak{B}}$ turn out to be comparable to the bound of Ref. 6. Thus a comparison of our results with those of Refs. 3 and 4 shows that we differ with them on two significant predictions about ω trajectory, namely (i) a large $\theta_{\omega\text{-}\mathfrak{B}}$ and (ii) a boost to the ω trajectory below threshold due to its mixing with $\mathfrak{B}$. Our considerations show that these specific claims of Refs. 3 and 4 arise, respectively, due to (i) an inconsistency in the treatment of several cylinder insertions which have the same threshold behavior and (ii) a misinterpretation of what the phenomenologically relevant ω trajectory below $b\bar{b}$ threshold should be. We have also studied the effects of incorporation of $b\bar{b}$ threshold in the work of Ref. 5 and we found that the resultant ω intercept and $\theta_{\omega\text{-}\phi}$, below $b\bar{b}$ threshold, are exactly the same as those of the CR model.[2] Thus as a result of the inclusion of the $b\bar{b}$ threshold, the model of Ref. 5 loses all the phenomenologically desirable features it had. No estimate of $\theta_{\omega\text{-}\mathfrak{B}}$ could be obtained from the trajectory intercepts below threshold as the two quantities get decoupled and above threshold there are more parameters than the available data can fix. However, for reasonable values of trajectory intercepts, the antiproton multiplicity data just above threshold seem to yield a bound on $\theta_{\omega\text{-}\mathfrak{B}}$, which is found to be consistent with the bound of Ref. 6.

The plan of our paper is as follows. In Sec. II, we show that the phenomenologically relevant ω and $\mathfrak{B}$ trajectories do not mix, below the $b\bar{b}$ threshold, in any DTU model of the Pomeron

which includes threshold effects for $b\bar{b}$ production. The ω trajectory which contains the admixture of $\mathcal{B}$ is shown to be relevant only at very high energies. In Sec. III, we confine ourselves to a one-dimensional model which has exact SU(3) symmetry and estimate in it $\theta_{\omega\text{-}\mathcal{B}}$, which with some reservations is found to be comparable with the bound of Ref. 6. In Sec. IV, we consider more realistic models with broken SU(3) symmetry. The estimates of $\theta_{\omega\text{-}\mathcal{B}}$ in these models are, indeed, found to be quite close to the bound of Ref. 6. The last section contains conclusions of our work.

II. $b\bar{b}$ threshold and ω-$\mathcal{B}$ mixing

Let us begin this section by considering a simple but illustrative example given by Dash *et al.*,[9] which, we hope, will be able to demonstrate the effects of thresholds in general. The physical insights, gained from this exercise, will be later employed in our discussion of ω-$\mathcal{B}$ mixing in the presence of the $b\bar{b}$ threshold. Let $P=1/(j-\alpha)$ and $C=ge^{-\mu j}$ be the planar propagator and the cylinder term, respectively. Then the renormalized propagator $P'=(P^{-1}-C)^{-1}$ can be written down, using this expression for P and C, in the following two exact and equivalent ways:

$$P'(j)=\frac{1}{j-\alpha-ge^{-\mu j}} \tag{1}$$

or alternatively,

$$P'(j)=\frac{1}{j-\alpha}+\frac{ge^{-\mu j}}{(j-\alpha)^2}+\frac{g^2e^{-2\mu j}}{(j-\alpha)^3}+\cdots. \tag{2}$$

Inverse Mellin transform of Eqs. (1) and (2) gives

$$P'(s)=\sum_i \beta_i\left(\frac{s}{s_0}\right)^{\alpha_i} \tag{3}$$

and

$$P'(s)=\left(\frac{s}{s_0}\right)^{\alpha}+\theta\left(\ln\frac{s}{s_0}-\mu\right)ge^{-\mu\alpha}\left(\frac{s}{s_0}\right)^{\alpha}\left(\ln\frac{s}{s_0}-\mu\right)+\theta\left(\ln\frac{s}{s_0}-2\mu\right)g^2\cdots, \tag{4}$$

where α_i satisfy $\alpha_i-\alpha-ge^{-\mu\alpha_i}=0$ and β_i is the residue of $P'(j)$ at α_i. Thus we see from Eqs. (3)–(4) that in the presence of a threshold for the cylinder kernel, the amplitude can be described in two equivalent ways. One way consists of using the infinite number of (mostly complex) renormalized poles as in Eq. (3), while the other involves use of only the unrenormalized pole with appropriate factors of $\ln(s/s_0)$, as in Eq. (4). It is also clear from these equations that in certain energy domains only one of these two ways will be convenient to use. Thus for $\ln(s/s_0)\gg\mu$, Eq. (3) will be an easier description to use, since Eq. (4) has lots of terms at these energies and Eq. (3) has only the leading pole term; the rest, being negligibly small, can be ignored. For $\ln(s/s_0)<\mu$, however, Eq. (4) is a better choice as it has only one term in this energy range, while Eq. (3) has many. Note, in particular, that for this energy region, the description of the amplitude in terms of only the leading pole in Eq. (3) is totally inadequate and the contribution of lower-lying poles has to be retained, as can be seen by comparing Eqs. (3) and (4) for $\ln(s/s_0)<\mu$. If one parametrizes the amplitude in terms of a single effective pole, as would be done in typical phenomenological analyses, then the considerations above tell us what the effective pole would look like. Thus writing

$$P'(s)=\beta_{\text{eff}}\left(\frac{s}{s_0}\right)^{\alpha_{\text{eff}}}, \tag{5}$$

we obtain

$$\alpha_{\text{eff}}=\alpha \quad \text{for} \quad \ln\frac{s}{s_0}<\mu$$

and

$$\alpha_{\text{eff}}\simeq\max\{\text{Re}\alpha_i\} \quad \text{for} \quad \ln\frac{s}{s_0}\gg\mu. \tag{6}$$

We see from Eq. (6) that (i) the phenomenologically relevant, effective pole does not get any boost below threshold and (ii) the leading pole in Eq. (3) coincides with the effective pole only at very high energies. By comparing Eqs. (4) and (5) just above threshold, we also note that above threshold $\alpha_{\text{eff}}>\alpha$, since the second term of Eq. (4), which arises due to the double pole term of Eq. (2), grows as $s^{\alpha}\ln s$.

Essentially the same arguments, as above, also imply that in any general DTU model, phenomenologically relevant ω and $\mathcal{B}$ trajectories do not mix below the $b\bar{b}$ threshold. The only difference is that ω-$\mathcal{B}$ mixing is a two-channel problem and, as we show below, this results in modifications of the couplings of these trajectories to external particles. Let us consider a typical DTU model of ω-$\mathcal{B}$ mixing in which threshold factors[10] for $b\bar{b}$ production are explicitly included so as to ensure agreement with the observed behavior of antiproton multiplicity data.[11] For the present, let us assume exact SU(3) symmetry.

Then the j-plane expression for the planar propagator of the model can be written down as

$$P=\begin{bmatrix}(j-\alpha_M)^{-1} & 0\\ 0 & (j-\alpha_E)^{-1}\end{bmatrix}, \tag{7}$$

where α_M and α_E are intercepts of planar $q\bar{q}$ and $qq\bar{q}\bar{q}$ trajectories (i.e., planar ω and $\mathcal{B}$), respectively. The values of α_M and α_E can be obtained

from bootstrap equations[3,12] or from Chew-Frautschi plots. The relevant graphs, which need to be included in the cylinder kernel of the renormalized propagator equation, are as shown in Fig. 1. The presence of the two planar graphs in Fig. 1, namely $B^{(2)}$ and $C^{(2)}$, is easily explained by noticing that α_M, α_E are supposed to be the solutions of planar bootstrap equations below the $b\bar{b}$ threshold and so do not include the contributions of planar graphs which have threshold. In terms of these diagrams, the cylinder kernel can be written down as below:

$$C^{\pm}=\begin{bmatrix} \pm(A)+(B^{(1)})+(B^{(2)}) & \sqrt{2}(C^{(1)})+\sqrt{2}(C^{(2)}) \\ \sqrt{2}(C^{(1)})+\sqrt{2}(C^{(2)}) & 2(D) \end{bmatrix}, \tag{8}$$

where the factors of $\sqrt{2}$ and 2 arise due to the two possible ways of stitching the diquark ends, and $\pm$ signs are for $C=\pm$ sector, respectively.[3] Let 2μ represent the rapidity threshold for production of a $b\bar{b}$ pair. Then it can be easily deduced that $B^{(1)}$ and $B^{(2)}$ have a threshold factor $e^{-2\mu j}$, while $C^{(1)}$, $C^{(2)}$ have a factor $e^{-\mu j}$ since, by cutting $B^{(1)}$, $B^{(2)}$ or a double iteration of $C^{(1)}$, $C^{(2)}$, one sees that they correspond to production of a $b\bar{b}$ pair. Displaying just this threshold behavior, Eq. (8) can be written

$$C^{\pm}=\begin{bmatrix} \pm A(j)+B(j)e^{-2\mu j} & \sqrt{2}C(j)e^{-\mu j} \\ \sqrt{2}C(j)e^{-\mu j} & 2D(j) \end{bmatrix}, \tag{9}$$

where A,B,C,D are functions of j, whose explicit form will be model dependent. As is clear from the notation, $A(j)$ and $D(j)$ represent the corresponding diagrams of Fig. 1, while $B(j)$ and $C(j)$ represent the sum of contributions of $B^{(1)}$, $B^{(2)}$ and $C^{(1)}$, $C^{(2)}$, respectively.

As is well known,[2] the renormalized propagator P'' can be written down in terms of P and C as

$$P''=(P^{-1}-C)^{-1}. \tag{10}$$

Splitting the kernel in two parts, as below,

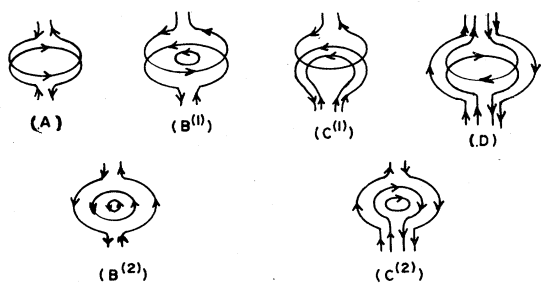

FIG. 1. The possible cylinder and planar graphs which need to be included in the cylinder kernel for the exact-SU(3) case.

$$C^{\pm}=C_0^{\pm}+C_1=\begin{bmatrix} \pm A(j) & 0 \\ 0 & 2D(j) \end{bmatrix} + \begin{bmatrix} B(j)e^{-2\mu j} & \sqrt{2}C(j)e^{-\mu j} \\ \sqrt{2}C(j)e^{-\mu j} & 0 \end{bmatrix}, \tag{11}$$

we rewrite Eq. (10) as

$$P''^{\pm}=(P^{-1}-C_0^{\pm}-C_1)^{-1} =[P_{\pm}'^{-1}-C_1]^{-1}, \tag{12}$$

where

$$P_{\pm}'=[P^{-1}-C_0^{\pm}]^{-1}. \tag{13}$$

It is clear from the definition of $P_{\pm}'$ above that the cylinder terms $C_0^{\pm}$ just renormalize the $q\bar{q}$ and $qq\bar{q}\,\bar{q}$ trajectories,[13] but do not mix them. Thus in most of the DTU models, the poles of $P_{\pm}'$ would be f which is pushed up to ~1, ω which is pushed down to ~0 or which is complex with $\mathrm{Re}\,\alpha\sim 0$, and $\mathfrak{B}^{\pm}$ which are pushed up; but these ω (f) and $\mathfrak{B}$ trajectories will be totally independent of each other, i.e., no ω-$\mathfrak{B}$ mixing will occur.

The form of Eq. (12) is now directly comparable to that of our simple example, considered above. Analogous to the P' there, P'' of Eq. (12) can also be described in the s plane in two exact and equivalent ways. We can use either the baryon-loop renormalized poles, whose intercepts satisfy the equation $\det(P_{\pm}'^{-1}-C_1)=0$ or the poles of $P_{\pm}'$. Again from our experience with the example, we know that the former will be more convenient at energies which are very high compared to the threshold, while the latter is more convenient at low energies. Therefore, for energies below or comparable to threshold, we expand Eq. (12) in an anologous manner to Eq. (2) and obtain

$$P''^{\pm}=P_{\pm}'+P_{\pm}'C_1P_{\pm}'+P_{\pm}'C_1P_{\pm}'C_1P_{\pm}'+\cdots. \tag{14}$$

For finding the effective renormalized poles below $b\bar{b}$ threshold, we retain in Eq. (14) only those terms which do not correspond to the production of one or more $b\bar{b}$ pairs. Therefore, as is clear from the diagrammatic representations of various terms in Eq. (14), all the iterations of $B^{(1)}$, $B^{(2)}$ and all but one iteration each of $C^{(1)}$, $C^{(2)}$ will have to be dropped from the equation. These terms, if retained, will have such θ functions in the s plane that the propagator will not get any contribution from them below the $b\bar{b}$ threshold. To illustrate further, again we draw an anology with our simple example, where for $\ln(s/s_0)<\mu$, an expression for P' could be obtained by dropping all but the first term of Eq. (2). Similarly, here the $P''^{\pm}$ has the following expression below the $b\bar{b}$ threshold:

$$P_b''^{\pm} \equiv \begin{bmatrix} P''^{\pm} \text{ below} \\ \text{threshold} \end{bmatrix} = P_{\pm}' + \begin{bmatrix} 0 & (P_{\pm}')_{11}(C_1)_{12}(P_{\pm}')_{22} \\ (P_{\pm}')_{22}(C_1)_{21}(P_{\pm}')_{11} & 0 \end{bmatrix}.$$

Substituting for $P_{\pm}'$ and C_1 in the above equation,

$$P_b''^{\pm} = \begin{bmatrix} \dfrac{1}{j-\alpha_M \mp A(j)} & \dfrac{\sqrt{2}C(j)e^{-\mu j}}{[j-\alpha_M \mp A(j)][j-\alpha_B-2D(j)]} \\ \dfrac{\sqrt{2}C(j)e^{-\mu j}}{[j-\alpha_M \mp A(j)][j-\alpha_B-2D(j)]} & \dfrac{1}{j-\alpha_B-2D(j)} \end{bmatrix}. \tag{15}$$

From Eq. (15), we clearly see that below threshold, $P''^{\pm}$ has only simple poles and they are at the same values of j as the poles of $P_{\pm}'$, i.e., they are given by

$$\begin{aligned} &j-\alpha_M \mp A(j)=0\,, \\ &j-\alpha_B-2D(j)=0\,. \end{aligned} \tag{16}$$

Of course, depending upon the model, $C(j)$ can have poles, but one expects these to be lower lying than the poles given by Eq. (16). This is due to the fact that singularities of $C(j)$ are governed by the baryon loop it has and baryon trajectories themselves have quite low intercepts. From Eq. (16) we clearly see that the poles of $P''^{\pm}$ below threshold are the renormalized but unmixed f, ω, and $\mathfrak{B}^{\pm}$ trajectories, which can be easily recognized as the phenomenologically relevant effective trajectories below threshold, by comparison with Eqs. (4) and (5). It may be mentioned here that a similar result was also obtained by Jones,[14] though in a physically different situation. Considering $K\bar{K}$ threshold in a broken SU(3) scheme, he too found that the phenomenologically relevant ω, ϕ do not mix below threshold. The basic arguments in our case are essentially the same as that of Jones.

As described earlier in the illustrative example, we can also describe the amplitude in terms of the poles of full $P''^{\pm}$, i.e., poles of $P''^{\pm}$ obtained by retaining all the terms in Eq. (14), which are given by the roots of the following equation:

$$\det(P_{\pm}'^{-1}-C_1)=\det(P^{-1}-C^{\pm})=0\,. \tag{17}$$

If $\{\alpha_i\}$ is the set of roots of Eq. (17), then in the s plane,

$$P''^{\pm}=\sum_i \beta_i^{\pm}\left(\frac{s}{s_0}\right)^{\alpha_i^{\pm}}, \tag{18}$$

where $\beta_i^{\pm}$ are residues of $P''^{\pm}(j)$ at $j=\alpha_i^{\pm}$ and the sum over i is an infinite sum, as α_i's are the complex roots of a transcendental equation.

From Eq. (18), it is clear that for energies which are very high compared to the threshold, one can drop the nonleading contributions and the amplitude can be adequately described in terms of only one or at least a few leading poles. Thus, as in the illustrative example, the phenomenologically observable effective trajectories at high energies will correspond to the leading poles of the set $\{\alpha_i^{\pm}\}$. We would like to emphasize that at energies below or comparable to $b\bar{b}$ threshold, the contribution of lower-lying poles is not negligible. Therefore a description in terms of only leading poles of $\{\alpha_i^{\pm}\}$ is inadequate at these energies. Exactly like the illustrative example, just above the $b\bar{b}$ threshold, $P''^{\pm}$ has double-pole terms due to the baryon-loop diagrams that have to be retained in $P''^{\pm}$ which we know will boost the leading trajectories (f,ω) by mixing them with nonleading ones $(\mathfrak{B}^{\pm})$. Thus, in short, the ω, f trajectories, as seen in phenomenological fits, have the following behavior in a typical DTU model. Below $b\bar{b}$ threshold they coincide with ω, f trajectories unrenormalized by baryon loops (unmixed with $\mathfrak{B}$). Above the $b\bar{b}$ threshold, they start getting boosted since more and more baryon loops are included as the energy increases, till at very high energies where they coincide with the leading baryon-loop renormalized trajectories (fully mixed with $\mathfrak{B}$).

Although, as argued above, the ω trajectory does not mix with $\mathfrak{B}$ below threshold, its physical coupling to any external baryons does become a mixture of planar ω coupling and planar $\mathfrak{B}$ coupling. To see this we just evaluate the residues of $P_b''^{-}$ at $j=\alpha_\omega$. The nontrivial contribution from the off-diagonal elements to the residue matrix will clearly have to be absorbed in the definition of physical ω coupling as it too would be a coefficient of $s^{\alpha_\omega-1}$ in the s plane. Since the off-diagonal elements couple to $\mathfrak{B}$ on one side, the physical ω coupling to baryons will depend on the planar $\mathfrak{B}$ coupling. Similarly, though by definition $\mathfrak{B}$ does not couple to mesons, due to the off-diagonal elements of Eq. (15) a nonzero baryonium contribution to meson-baryon scattering is possible. It is these effects which can give rise to a nonzero "ω-$\mathfrak{B}$ mixing angle" (the quotes are to remind us that this is simply the analog of the angle defined in Ref. 6).

It is quite straightforward to generalize these considerations to the DTU models where SU(3) is

broken and convince oneself that the basic results about the renormalization effects due to baryon loops are essentially the same. In fact, apart from simplifying our equations, the SU(3) symmetry was not used anywhere in our arguments.

III. AN SU(3)-SYMMETRIC MODEL

In this section we present a model which is based on the one-dimensional approximation scheme of Kwiecinski and Sakai[8] and which has identical assumptions as those of Ref. 3. However, our results are entirely different for reasons which will be elaborated below.

The basic assumptions of the model are (i) SU(3) is exact, and (ii) all exotic meson and exotic baryon exchanges in loops are ignored.

As is well known, the first step in the scheme of Ref. 8 consists of solving the bootstrap equation at planar level, which then fixes almost all the parameters at the cylinder level. The bootstrap equations for ordinary ($q\bar{q}$) mesons and baryoniums ($qqq\bar{q}\bar{q}$) can be formulated and solved in this model exactly the same way as in Ref. 3. The solutions, as obtained in Ref. 3, are

$$\alpha_E = -0.7, \quad \bar{\alpha}_M = -0.075, \quad \bar{\alpha}_B = -0.675,$$
$$g_1^2 = g_3^2 = 0.31, \tag{19}$$

where the following inputs have been used:

$$\alpha_M = 0.5, \quad \alpha_B = -0.1, \quad \bar{x} = 2.3. \tag{20}$$

Here $\alpha_{M,B,E}$ are the intercepts of planar $q\bar{q}$, qqq, and $qqq\bar{q}\bar{q}$ trajectories, respectively, and the corresponding $\bar{\alpha}$'s are their appropriate average values over the transverse motion.[8] g_1 and g_3 are couplings, as shown in Fig. 2, and $\bar{x}$ represents the maximum spread in rapidity of the resonant clusters.

Let us now consider the nonplanar insertions along with those planar insertions which contribute only above the $b\bar{b}$ threshold. The general form of the kernel for the renormalized propagator equation has already been written down in Eq. (9). Following Ref. 8, we can write down the following expressions for various terms of Eq. (9)

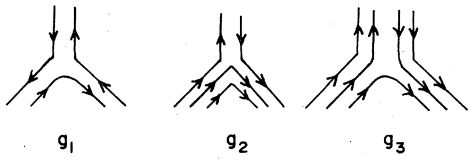

FIG. 2. Regge couplings.

(Ref. 15):

$$A(j) = \frac{3g_1^2}{j - 2\bar{\alpha}_M + 1}, \quad B(j) = \frac{18g_2^2 \exp(2\mu\alpha_M)}{j - 2\bar{\alpha}_B + 1},$$
$$C(j) = \frac{6\sqrt{3}g_2 g_3 \exp(\mu\alpha_M)}{j - 2\bar{\alpha}_B + 1}, \quad D(j) = \frac{3g_3^2}{j - 2\bar{\alpha}_B + 1}, \tag{21}$$

where g_2 is the Reggeon-baryon-antibaryon coupling shown in Fig. 2 and μ has already been defined in Sec. II.

Using Eqs. (16), which involve only A and D of Eq. (21), and the values of various parameters from Eqs. (19)–(20), we obtain the following intercepts for phenomenologically relevant f, ω, and $\mathfrak{B}^*$ trajectories below the $b\bar{b}$ threshold:

$$\alpha_f^{(1)} = 0.95, \quad \alpha_\omega^{(1)} = -0.33 + 0.53i, \quad \alpha_{\mathfrak{B}^*}^{(1)} = 0.08. \tag{22}$$

We know from Sec. II that these values of j correspond to the positions of poles of both $P'_\pm$ and $P''^\pm_b$ which are defined by Eqs. (13) and (15), respectively. Calculating the residues at these pole positions, we find that the residues of $P'_\pm$ are

$$\rho_f^{(1)} = 0.82, \quad \rho_\omega^{(1)} = 0.5 - 0.77i, \quad \rho_{\mathfrak{B}^*}^{(1)} = 0.75, \tag{23}$$

where $\rho_i^{(1)}$ is also the ratio of the Regge residues of the renormalized trajectory i and its corresponding planar trajectory.[16] The residue of $P''^\pm_b$ at each of these poles is, however, a matrix, which in general has nonzero off-diagonal elements. From Eq. (15) we clearly see that a diagonal element of any of these residue matrices is either the appropriate $\rho_i^{(1)}$ or zero. Introducing a "mixing angle" "θ_i" (the quotes are to distinguish it from a genuine mixing angle that characterizes mixing between states), we can parametrize the off-diagonal elements of residue matrix. Thus, for ω residue matrix, we write[17]

$$\text{res}(P''^- \text{ below threshold})\Big|_{j=\alpha_\omega} = \begin{bmatrix} \rho_\omega^{(1)} & \sqrt{\rho_\omega^{(1)}}\sin\text{“}\theta_\omega\text{”} \\ \sqrt{\rho_\omega^{(1)}}\sin\text{“}\theta_\omega\text{”} & 0 \end{bmatrix}. \tag{24}$$

Similarly, the $\mathfrak{B}^-$ residue matrix can be written down in terms of $\rho_{\mathfrak{B}^-}$ and "$\theta_{\mathfrak{B}^-}$". Clearly these "θ_i", which characterize the mixing effects in couplings, depend on both g_2 and μ, which cannot be fixed from any consistency equation in the present scheme. So following Ref. 3, we obtain these parameters by fitting $\langle n_{\bar{p}} \rangle$ data. In Appendix A, we derive an expression for $\langle n_{\bar{p}} \rangle$ just above threshold. By fitting it to the data of Antinucci *et al.*,[11] near $s \sim 100$ GeV^2, we obtain

$$g_2 = 0.075 \pm 0.02, \quad \mu = 0.63 \pm 0.02. \tag{25}$$

Having thus known g_2 and μ, we can easily calculate the various "θ_i" by comparing the residue

of $P''^{\pm}$ below threshold at $j=\alpha_i$, obtained from Eq. (15), with Eq. (24). However, instead of doing so, we will obtain the estimate of a quantity, called the ω-$\mathcal{B}$ mixing angle "$\theta_{\omega\text{-}\mathcal{B}}$", which is related to these "θ_i", and compare it with the existing phenomenological bound of Ref. 6 which is as stated below:

$$|\sin^2\text{“}\theta_{\omega\text{-}\mathcal{B}}\text{”}| \lesssim 0.067 \quad \text{or} \quad |\text{“}\theta_{\omega\text{-}\mathcal{B}}\text{”}| \lesssim 15^\circ . \tag{26}$$

As shown in Appendix B, this $\sin^2$"$\theta_{\omega\text{-}\mathcal{B}}$" is simply proportional to $\sin$"θ_ω" $\sin$"$\theta_{\mathcal{B}}$" in our model. Substituting the values given by Eqs. (19), (20), (22), (23), and (25) in Eq. (B6) of the Appendix, we get the following value for it;

$$\sin^2\text{“}\theta_{\omega\text{-}\mathcal{B}}\text{”} = 0.146 - 0.039i . \tag{27}$$

The complex value of "$\theta_{\omega\text{-}\mathcal{B}}$", appearing in the equation above, should not surprise us, since below $b\bar{b}$ threshold the effective ω trajectory is itself complex. Ignoring the small imaginary part of Eq. (27), however, we obtain

$$\text{“}\theta_{\omega\text{-}\mathcal{B}}\text{”} = 22.4^\circ , \tag{28}$$

which appears quite comparable to the bound, particularly if one notes that $\mathrm{Re}\alpha_\omega(0)$ is quite low in this model.

As we showed in Sec. II, there is an alternative way of describing the amplitude in this model, and it is in terms of the poles of a full propagator whose intercepts are given by roots of Eq. (17). Substituting values of P and C and solving Eq. (17), we obtain the following values for the intercepts of leading poles (i.e., with largest $\mathrm{Re}\alpha$):

$$\alpha_f^{(2)} = 0.97, \quad \alpha_\omega^{(2)} = 0.25 . \tag{29}$$

The residue of the full propagator $P''^{\pm}$ at these poles can be written as below:

$$\mathrm{res}P''^{\pm}\Big|_{j=\alpha_i} = \rho_i^{(2)} \begin{bmatrix} \cos^2\theta_i^{(2)} & \sin\theta_i^{(2)}\cos\theta_i^{(2)} \\ \sin\theta_i^{(2)}\cos\theta_i^{(2)} & \sin^2\theta_i^{(2)} \end{bmatrix} , \tag{30}$$

where these (ρ_i, θ_i) define the renormalized states in terms of the planar states. Thus, for example, renormalized f is given by

$$|f\rangle = \rho_f^{(2)}[\cos\theta_f^{(2)}|f^P\rangle + \sin\theta_f^{(2)}|\mathcal{B}^{(+)P}\rangle] . \tag{31}$$

The values of these residue parameters can be easily calculated by comparing the residue of $P''^{\pm}$ at a pole with Eq. (30). For the leading poles, we obtain

$$\begin{aligned} &\rho_f^{(2)} = 0.79, \quad \theta_f^{(2)} = 9.93^\circ , \\ &\rho_\omega^{(2)} = 0.78, \quad \theta_\omega^{(2)} = 52.5^\circ . \end{aligned} \tag{32}$$

Thus we see that the f trajectory in this model is affected very little due to baryon-loop renormalization, but the ω trajectory, which had a complex intercept at low energies becomes real and gets boosted to 0.25 at very high energies as a result of strong ω-$\mathcal{B}$ mixing.

Before closing this section, we would like to compare and contrast our results with those of Chan and Tsou[3] who, based on exactly the same assumptions as above, had claimed entirely different physical results. Thus in their model, the ω trajectory had a reasonable intercept 0.37, below the $b\bar{b}$ threshold[18] [solution with superscript (2) in their notation], due to strong ω-$\mathcal{B}$ mixing ($\theta_{\omega\text{-}\mathcal{B}} \sim 50^\circ$) while above threshold [solution (3)] f got boosted to 1.04, which was a welcome feature for explaining the rising total cross-section data. Our considerations above show that these results are incorrect for the following reasons.

Noting that their solution (2) consists of simply the leading poles of the infinite series of complex renormalized poles, we immediately see that their claim about boost of ω below threshold is based on a misinterpretation of what the phenomenologically relevant ω trajectory in that energy range should be. As we saw in Sec. II, these leading trajectories can be adequate for describing the amplitude only at high energies but they are certainly inadequate, and therefore phenomenologically meaningless, at low energies such as below $b\bar{b}$ threshold. The solution (2) also suffered from an inconsistency of treatment of the cylinder diagrams B and C^2 (i.e., a double iteration of C), which have identical threshold behavior but of which only C^2 and its higher iterations (along with other higher iterations of C) were retained in solution (2). Therefore, even for high energies, solution (2) is not valid.

The same inconsistency of differentiating between B and C^2 diagrams has also resulted in Ref. 3 in an incorrect value of the parameter g_2, which crucially governs the amount of ω-$\mathcal{B}$ mixing. Thus while calculating an expression for $\langle n_{\vec{p}} \rangle$ just above threshold, which was later fitted with the data of Ref. 11 to obtain g_2, contributions of C^2 terms were not included in Ref. 3. This contribution turns out to be as sizable as the one that had been included and in fact, as our calculation shows, g_2 goes down by a factor of ~3 as a result of inclusion of these terms. Using this value of g_2 one finds that the $f, \mathcal{B}$ trajectories receive a smaller boost above threshold than what was mentioned in Ref. 3. In particular, we find that $\alpha_f(0) < 1$, so that rising cross sections cannot be explained in this model. The smaller value of g_2 also yields a smaller ω-$\mathcal{B}$ mixing angle below threshold. Finally, we note that our solution below $b\bar{b}$ threshold is the same as solution (1) of Ref. 3, except for the coupling modifications. Of

course, the solution (1) was not regarded as the physical solution in Ref. 3. Our solution above threshold is similar to their solution (3), but the numerical results are different due to the above-mentioned difference in the estimate of g_2.

IV. BROKEN-SU(3) MODELS

As remarked earlier in Sec. II, the case of broken-SU(3) models is very similar to that of SU(3)-symmetric models and hence all the conclusions obtained there can be obtained here also in an analogous fashion. We will, therefore, content ourselves in making this similarity clearer in a brief manner, which will also help us in establishing our notation for this section. We then proceed to more detailed consideration of specific models.

The planar propagator in the j plane for a general DTU model of ω-ϕ-$\mathfrak{G}$ mixing can be written down as

$$P=\begin{bmatrix}(j-\alpha_\rho)^{-1} & 0 & 0\\ 0 & (j-\alpha_\phi)^{-1} & 0\\ 0 & 0 & (j-\alpha_E)^{-1}\end{bmatrix}, \tag{33}$$

where α_ρ, α_ϕ, and α_E are intercepts of planar ρ, ϕ, and $\mathfrak{G}$ trajectories, respectively. As is clear from the equation above, we have chosen to ignore SU(3)-breaking effects in the baryonium sector as we feel that they will be negligible due to the heaviness of the strange quark.

The relevant cylinder (and also some planar) diagrams which are analogs of the diagrams of Fig. 1 are shown in Fig. 3. In terms of these the analog of Eq. (9) of Sec. II can be easily written down as below:

$$C^{\pm}=\begin{bmatrix}\pm 2A_\rho+6B_\rho e^{-2\mu j} & \pm\sqrt{2}A_{K^*}+3\sqrt{2}B_{K^*}e^{-2\mu j} & 6C_\rho e^{-\mu j}\\ \pm\sqrt{2}A_{K^*}+3\sqrt{2}B_{K^*}e^{-2\mu j} & \pm A_\phi+3B_\phi e^{-2\mu j} & 3\sqrt{2}\,C_\phi e^{-\mu j}\\ 6C_\rho e^{-\mu j} & 3\sqrt{2}\,C_\phi e^{-\mu j} & 6D\end{bmatrix} \tag{34}$$

where as before A_M, B_M, C_M, D for $M=\rho, K^*, \phi$ are functions of j, which represent the corresponding diagrams[19] and whose explicit form will be model dependent.

Splitting $C^{\pm}$ in μ-dependent and μ-independent parts and proceeding along the lines of Sec. II, one can easily show that (i) below the $b\bar{b}$ threshold the phenomenologically relevant ω, ϕ (f, f') trajectories, whose intercepts are given by leading roots of the equation

$$(j-\alpha_\rho \pm 2A_\rho)(j-\alpha_\phi \pm 2A_\phi)-2A_{K^*}{}^2=0, \tag{35}$$

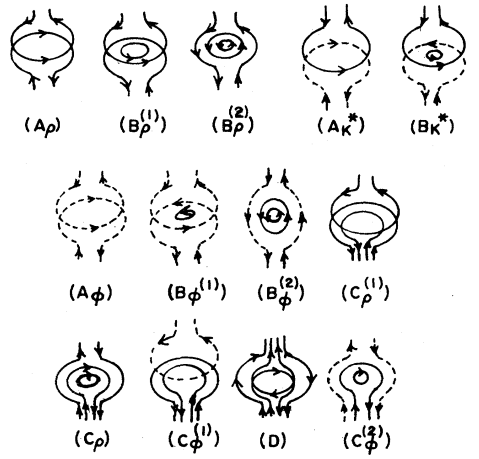

FIG. 3. Same as Fig. 1, but for the broken-SU(3) case.

do not mix with the $\mathfrak{G}^-$ ($\mathfrak{G}^+$) trajectory whose intercept is given by the leading root of the equation

$$j-\alpha_E-2D=0, \tag{36}$$

and (ii) the couplings of these trajectories do undergo a modification and so a nontrivial "$\theta_{\omega\text{-}\mathfrak{G}}$" is possible below the $b\bar{b}$ threshold.

Finally, we note that if α is the leading root of Eq. (35), then by rotating the basis of matrices P, C from $|u\bar{u}\rangle$, $|d\bar{d}\rangle$, $|qq\bar{q}\bar{q}\rangle$ to $|\alpha\rangle$, $|\beta\rangle$, $|qq\bar{q}\bar{q}\rangle$, where $|\beta\rangle$ is orthogonal to $|\alpha\rangle$, we can cast $C^{\pm}$ in an effective 2×2 matrix form for a calculation which retains only leading pole contributions in $q\bar{q}$ sector. Then the calculations of $\langle n_{\vec{p}}\rangle$ and "$\theta_{\omega\text{-}\mathfrak{G}}$" in a broken-SU(3) model are also analogous to those in exact-SU(3)-symmetry model, presented in Appendices A and B, respectively.

Let us now turn to specific models.

(*i*) *Model A.* This model is quite similar to the one considered in Sec. III, except that here we will consider the ordinary meson sector with broken SU(3) and hence this model is more realistic. Our assumptions now will be identical to those of Ref. 4. In particular, all the couplings are assumed to be SU(3) symmetric, which simplifies the $(q\bar{q})$ meson bootstrap equations and one can readily solve them, as in Ref. 4. The solutions, as obtained in Ref. 4, are

$$2\bar{\alpha}_M=\alpha_M-0.65 \quad \text{for } M=\rho, K^*, \phi \quad \text{and} \quad g_1{}^2=0.38, \tag{37}$$

where following input parameters were used:

$$\alpha_\rho = 0.5,\ \alpha_{K^*} = 0.35,\ \alpha_\phi = 0.2,\ \bar{\varkappa} = 2.3,$$
$$N_{eff} = \text{effective number of flavors} = 2.5. \tag{38}$$

Since exact SU(3) is assumed in the baryonium sector, the solution of baryonium bootstrap equation remains the same as in Sec. III.

Turning to the cylinder corrections, the explicit j dependence of the functions in Eq. (34) can be written down as in Sec. III,

$$A_M = \frac{g_1^2}{j - 2\bar{\alpha}_M + 1},\quad B_M = \frac{n_1 g_2^2 \exp(2\mu\alpha_M)}{j - 2\bar{\alpha}_{\mathfrak{B}} + 1}$$
$$C_M = \frac{2 g_2 g_3 \exp(\mu\alpha_M)}{j - 2\bar{\alpha}_B + 1},\quad D = \frac{g_3^2}{j - 2\bar{\alpha}_B + 1}, \tag{39}$$

where $n_1 = 2$ for $M = \rho, \phi$, and 1 for $M = K^*$. Substituting A_M and D, defined above, in Eqs. (35) and (36) and using the already specified values of the parameters, one easily obtains the intercepts of $f, \omega, \ldots$ trajectories below the $b\bar{b}$ threshold. One can then calculate the residues of P' which in the present model can be defined by an equation analogous to Eq. (13). Unlike in Sec. III, the residue of P' at $j = \alpha_i$, for an ordinary meson pole α_i, is a matrix which can be written down in terms of two parameters ρ_i, θ_i as follows:

$$\text{res}P'\,|_{j=\alpha_i} = \rho_i^{(1)} \begin{bmatrix} \cos^2\theta_i^{(1)} & \sin\theta_i^{(1)}\cos\theta_i^{(1)} & 0 \\ \sin\theta_i^{(1)}\cos\theta_i^{(1)} & \sin^2\theta_i^{(1)} & 0 \\ 0 & 0 & 0 \end{bmatrix}.$$

We list in Table I the values of intercepts and residue parameters of leading cylinder-renormalized trajectories below $b\bar{b}$ threshold. As one sees from Table I, the f and ω trajectories have acquired reasonable intercepts below threshold through mixing with $s\bar{s}$, although the boost to ω is a little below the phenomenologically desirable level. The similarity of these results with those of Tsou[20] is also remarkable, particularly since her model had included the effects of transverse momenta which were neglected in the present model.

As in Sec. III, the values of g_2 and μ, which are needed to estimate "$\theta_{\omega\text{-}\mathfrak{B}}$" and the parameters of leading trajectories at very high energies, can be obtained by fitting $\langle n_{\bar{p}} \rangle$ data. The expression for $\langle n_{\bar{p}} \rangle$ in terms of model parameters is given in Appendix A by Eqs. (A3), and (A5). Fitting it to the data of Ref. 11, we obtain

$$g_2 = 0.086 \pm 0.02,\quad \mu = 0.67 \pm 0.05. \tag{40}$$

Now values of all the parameters are specified and therefore one can easily calculate "$\theta_{\omega\text{-}\mathfrak{B}}$" in this model by using the expression given by Eq. (B7):

$$\sin^2\text{"}\theta_{\omega\text{-}\mathfrak{B}}\text{"} = 0.103 \pm 0.034 \quad \text{or} \quad \text{"}\theta_{\omega\text{-}\mathfrak{B}}\text{"} = 18.7^\circ \pm 3.2^\circ,$$

which is indeed close to the phenomenological bound of Ref. 6. It may also be mentioned here that if in a model $\alpha_\omega^{(1)}$ or $\alpha_{\mathfrak{B}}^{(1)}$ turns out to be closer to its phenomenologically favored value than that in Table I, then the estimate above will go down further.

Finally, solving the equations $\det[P^{-1} \pm C] = 0$, we obtain the intercepts of trajectories relevant at very high energies. For the leading trajectories in $C = \pm$ sectors these intercepts are

$$\alpha_f = 0.98,\quad \alpha_\omega = 0.36.$$

Comparing these values with those in Table I, we note that as in Sec. III the baryon-loop corrections have caused very little change in the f and ω intercepts.

Once again our results can be contrasted with those of a model[4] which was based on identical assumptions as ours, but which had predicted a substantial boost to the ω trajectory and a large ω-$\mathfrak{B}$ mixing angle ("$\theta_{\omega\text{-}\mathfrak{B}}$" $\sim 42^\circ$) below $b\bar{b}$ threshold. Again one can show that as in Ref. 3, these claims arise due to (i) misinterpretation of what the effective trajectories below threshold should be and (ii) the inconsistent treatment of cylinder diagrams B and C. Since we have already elaborated on these points in Sec. III, we will not repeat them here.

(ii) Model B. This is based on the phenomenological approach of Chew and Rosenzweig[2] and Gavai[5] in which instead of fixing the cylinder terms from the planar bootstrap equation they are treated as free parameters. Following Refs. 2 and 5, we assume SU(3) symmetry and j independence for

TABLE I. The values of intercepts and residue parameters of leading cylinder renormalized trajectories below $b\bar{b}$ threshold.

$C = +$ sector	$C = -$ sector
$\alpha_f^{(1)} = 0.96,\ \rho_f^{(1)} = 0.8,\ \theta_f^{(1)} = 21.54^\circ$	$\alpha_\omega^{(1)} = 0.33,\ \rho_\omega^{(1)} = 1.03,\ \theta_\omega^{(1)} = -43.8^\circ$
$\alpha_{f'}^{(1)} = 0.27,\ \rho_{f'}^{(1)} = 1.01,\ \theta_{f'}^{(1)} = 113.8^\circ$	$\alpha_\phi = -0.43 + 0.67i$
$\alpha_{\mathfrak{B}}^{(1)} = 0.08,\ \rho_{\mathfrak{B}}^{(1)} = 0.75$	$\alpha_{\mathfrak{B}}^{(1)} = 0.08,\ \rho_{\mathfrak{B}}^{(1)} = 0.75$

the kernel [i.e., all SU(3) breaking is included in $\alpha_\rho \neq \alpha_\phi$]. Then it is easy to deduce that the kernel $C^{\pm}$ of Eq. (34) can be described in terms of four parameters, say, k_0, k_1, k_2, k_3,

$$D = k_2 \text{ and } A_M = k_0,\ B_M = k_3,\ C_M = k_1 \quad \text{for } M = \rho, K^*, \phi. \quad (41)$$

Substituting for A_M and D in Eqs. (35) and (36) and solving these equations, we see that the effective f, ω intercepts below threshold have exactly the same expression as in the CR model,[2] i.e., the amount of ω-ϕ mixing and the ω-trajectory renormalization for a given set of input parameters is unchanged. Thus, this more realistic consideration of baryon exchanges by incorporating $b\bar{b}$ thresholds, compared to that of Ref. 5, has turned out to be of no use for the two problems which the CR model had, and which Ref. 5 seemed to overcome.

One would then like to know whether there are any gains from incorporating $\mathcal{B}$ mixing at all. Apart from being able to explain the possible deviations below $b\bar{b}$ threshold in some couplings such as $\omega b\bar{b}$, $\mathcal{B}MM$ (where M is an ordinary meson), the incorporation of $\mathcal{B}$ mixing also seems to have one possible attractive feature which is the following. Since the leading trajectories in both $C = \pm$ sectors will be boosted above the $b\bar{b}$ threshold due to mixing with $\mathcal{B}$, the f, ω contributions to the cross sections above threshold will fall less steeply than below threshold. The f contribution can even rise above certain energies. Thus it may be possible in this model to fit the total-cross-section data over a wider range where such a behavior is known to be existing. To check whether this is indeed the case, we must find out the poles of $P'' = (P^{-1} - C)^{-1}$ and for that we need values of five parameters of our model, namely α_E, k_1, k_2, k_3, and μ, as the values of remaining parameters, i.e., $\alpha_\rho, \alpha_\phi, k_0$ can be fixed from total-cross-section data below 30 GeV/c.[21] However, noting that in P'', α_E and k_2 occur only in the combination $(\alpha_E + 6k_2)$, which in the present model is the intercept of physical baryonium below threshold, we see that we have effectively only four parameters. Of these, $\alpha_{\mathcal{B}}$, i.e., the intercept of physical baryonium below threshold, can be obtained from fits to total or inclusive cross-section differences,[22,6] while μ, the threshold parameter, can be fixed from the antiproton multiplicity data of Antinucci *et al.*[11] The same multiplicity data also gives a constraint on k_1 and k_3, which can fix the value of k_3 since one can determine k_1 from the value of "$\theta_{\omega\text{-}\mathcal{B}}$" which in turn may be obtained from an analysis similar to that of Ref. 6, but of presumably better data. Thus it seems possible to obtain all the parameters of the model from data and check whether $\alpha_f(0) > 1$ above threshold. However, the poor quality of the currently available data prevents us from undertaking such an exercise, as the resultant uncertainties in various parameters are unlikely to lead to any definite conclusion. The data can, however, put a reasonable bound on "$\theta_{\omega\text{-}\mathcal{B}}$", which we proceed to obtain now.

From the expression for $\sin^2$"$\theta_{\omega\text{-}\mathcal{B}}$" in this model, given by Eq. (B8), we note that we need values of k_1 and μ in order to estimate "$\theta_{\omega\text{-}\mathcal{B}}$" as the rest of the parameters can be obtained from fits to total and inclusive cross sections.[21,22,6] Once again we determine k_1 and μ by fitting $\langle n_{\bar{p}} \rangle$ data to the model expression, given by Eq. (A6). Note that $\langle n_{\bar{p}} \rangle$ depends on k_3 also. But since $k_3 \geq 0$ at $t = 0$, we put $k_3 = 0$ and obtain maximum possible value for k_1,

$$k_1 = 0.034 \pm 0.008, \quad \mu = 0.76 \pm 0.01,$$

where we have used $\alpha_{\mathcal{B}}^{(1)} = -1$ and the values of Ref. 21 for $\alpha_f^{(1)}, \theta_f^{(1)}$. Substituting the values of k_1, μ in Eq. (B8) and using $\alpha_\omega^{(1)}, \theta_\omega^{(1)}$ from Ref. 21, we obtain

$$\sin^2\text{"}\theta_{\omega\text{-}\mathcal{B}}\text{"} = 0.03 \pm 0.014 \quad \text{or} \quad \text{"}\theta_{\omega\text{-}\mathcal{B}}\text{"} = 9.9^\circ \pm 2.4^\circ.$$

Since this estimate was for largest possible k_1 we see that $\langle n_{\bar{p}} \rangle$ data gives a bound on "$\theta_{\omega\text{-}\mathcal{B}}$", namely $|\text{"}\theta_{\omega\text{-}\mathcal{B}}\text{"}| < 12.5^\circ$, which agrees reasonably well with the phenomenological bound of Ref. 6.

V. CONCLUSIONS

In this paper, we have investigated in detail a general class of DTU models of Pomeron in which ω- mixing is considered in the presence of the $b\bar{b}$ threshold. We have shown that the phenomenologically relevant ω (f) and $\mathcal{B}^-$ ($\mathcal{B}^+$) trajectories in these models do not mix below threshold and therefore ω-$\mathcal{B}$ mixing cannot be invoked to cure problems of ω trajectory for $s \lesssim 100$ GeV^2. This result arises simply due to the fact that no internal baryon loop which has only mesonic legs is permissible below $b\bar{b}$ threshold in the unitarity sum. The only baryonic loop which is allowed in this energy range has a baryonium and an ordinary meson as its legs. We have shown that this loop can only modify the couplings of $\omega, \mathcal{B}^-$ trajectories (also of $f, \mathcal{B}^+$ trajectories) to external particles and thus it can in general give rise to a nontrivial "$\theta_{\omega\text{-}\mathcal{B}}$", which is the analog of the quantity on which Gavai and Roy[6] had obtained a phenomenological bound. We have also shown that the f, ω trajectories which have admixture of $\mathcal{B}^-, \mathcal{B}^+$, respectively, can be used to describe the amplitude only at very high energies, but they are certainly inadequate at low energies.

Turning to explicit model considerations, we studied three models and verified all the statements made above in each of them. One of these models had exact SU(3) symmetry and was based on essentially the same assumptions as that of Chan and Tsou,[3] while the other two had broken SU(3) in ordinary meson sector and were based on assumptions similar to those of Gavai[5] and Hansson.[4] We found that in the model with exact SU(3) symmetry, the ω trajectory below threshold had a complex intercept with $\mathrm{Re}\alpha_\omega \sim -0.3$. The estimation of "$\theta_{\omega\text{-}\mathcal{B}}$" in this model, i.e., ω-$\mathcal{B}$ mixing angle below threshold, yielded a complex value. Ignoring the small imaginary part of it, "$\theta_{\omega\text{-}\mathcal{B}}$" $\simeq 22.4°$. These results were in sharp contrast with those of Ref. 3, which had claimed $\alpha_\omega(0) \simeq 0.37$ and "$\theta_{\omega\text{-}\mathcal{B}}$" $\simeq 50°$ below $b\bar{b}$ threshold. Our considerations showed that these two claims in Ref. 3 arose due to (i) a misinterpretation of what the phenomenologically relevant ω trajectory below $b\bar{b}$ threshold should be and (ii) an inconsistent treatment of two sets of cylinder diagrams that had the same threshold behavior.

Attempts to include $b\bar{b}$ threshold effects in the work of Ref. 5 seemed to eliminate the phenomenologically desirable feature it had, as below the threshold the model became almost identical to the CR model[2] except that a nonzero "$\theta_{\omega\text{-}\mathcal{B}}$" was explicable in it. Using the $\langle n_p \rangle$ data to determine some of the model parameters, we found that for reasonable values of input intercepts, the allowed range of "$\theta_{\omega\text{-}\mathcal{B}}$" in the model, which is given by $|\text{"}\theta_{\omega\text{-}\mathcal{B}}\text{"}| \lesssim 13°$, was consistent with the bound of Ref. 6. In the other broken-SU(3) model, where most of the parameters were determined from bootstrap constraints, we found that the ω trajectory below threshold had a not so unreasonable intercept ~0.33 due to ω-ϕ mixing. The predicted value of "$\theta_{\omega\text{-}\mathcal{B}}$" in the model was ~19°, which is remarkably close to the bound of Ref. 6 and is expected to be still closer if $\alpha_\omega(0)$ acquires a phenomenologically favorable value.

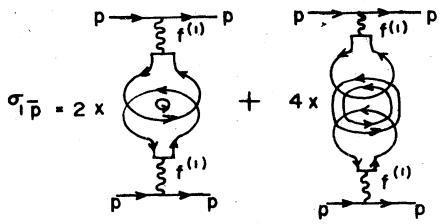

FIG. 4. Diagrammatic representation of one-antiproton-production cross section.

ACKNOWLEDGMENTS

I wish to thank Dr. D. P. Roy for suggesting this problem. I would also like to thank him and Professor J. Kwiecinski for stimulating discussions. A correspondence with Professor H. M. Chan is gratefully acknowledged.

APPENDIX A

In this appendix, we briefly describe how to derive the expression for the antiproton multiplicity $\langle n_{\bar{p}} \rangle$ in pp collisions in the exact SU(3) model of Sec. III. Also, we list the corresponding expressions for the broken-SU(3) models. As pointed out in Ref. 3, all the contribution to $\langle n_{\bar{p}} \rangle$ at energies just above $b\bar{b}$ threshold must come from $\sigma_{1\bar{p}}$, i.e., one-antiproton-production cross section. The leading-pole contribution to $\sigma_{1\bar{p}}$ is diagrammatically shown in Fig. 4. The factors 2 and 4 are simply due to the fact that in the present one-dimensional scheme the diagrams $B^{(1)}$ and $C^{(1)}$ of Fig. 1 have the same contribution as $B^{(2)}$ and $C^{(2)}$, respectively.

The j-plane expression for $\sigma_{1\bar{p}}$ can therefore be written as

$$\sigma_{1\bar{p}} = \frac{\rho_f^{(1)}}{(j-\alpha_f^{(1)})^2}\left[(\gamma_p^f)^P e^{-\mu(j-1)} + \frac{6\sqrt{6}g_2 g_3 \rho_{\mathcal{B}}^{(1)}(\gamma_p^{\mathcal{B}})^P e^{-\mu(j-\alpha_M)}}{(j-\alpha_{\mathcal{B}}^{(1)})(j-2\bar{\alpha}_B+1)}\right]^2 \left[\frac{18 g_2^2 e^{-2\mu(j-\alpha_M)}}{j-2\bar{\alpha}_B+1} + \frac{216 g_2^2 g_3^2 \rho_{\mathcal{B}}^{(1)} e^{-2\mu(j-\alpha_M)}}{(j-\alpha_{\mathcal{B}}^{(1)})(j-2\bar{\alpha}_B+1)}\right], \quad \text{(A1)}$$

where superscript P stands for planar. Noting that the zero-antiproton-production cross section $\sigma_{0\bar{p}}$ is given by

$$\sigma_{0\bar{p}} = \frac{\rho_f^{(1)}}{j-\alpha_f^{(1)}}\left[(\gamma_p^f)^P e^{-\mu(j-1)} + \frac{6\sqrt{6}g_2 g_3 \rho_{\mathcal{B}}^{(1)}(\gamma_p^{\mathcal{B}})^P e^{-\mu(j-\alpha_M)}}{(j-\alpha_{\mathcal{B}}^{(1)})(j-2\bar{\alpha}_B+1)}\right]^2 \quad \text{(A2)}$$

and using[23] $\langle n_{\bar{p}} \rangle \simeq \sigma_{1\bar{p}}/2\sigma_{0\bar{p}}$ near threshold, we obtain

$$\langle n_{\bar{p}} \rangle = \frac{9\rho_f^{(1)} g_2^2 e^{-2\mu(\alpha_f^{(1)}-\alpha_M)}}{\alpha_f^{(1)}-2\bar{\alpha}_B+1}\{(Y-4\mu)(c+b) - (1+a)^{-2}[(\alpha_f^{(1)}-2\bar{\alpha}_B+1)^{-1}(c+2b+4ac+6ab+3a^2c+4a^2b) + (\alpha_f^{(1)}-\alpha_{\mathcal{B}}^{(1)})^{-1}(b+2ac+4ab+2a^2c+3a^2b)]\}, \quad \text{(A3)}$$

where $Y=\ln(s/s_0)$ and

$$a=\frac{6\sqrt{6}g_2g_3\rho_{\mathfrak{B}}^{(1)}e^{-\mu(1-\alpha_M)}}{(\alpha_f^{(1)}-\alpha_{\mathfrak{B}}^{(1)})(\alpha_f^{(1)}-2\bar{\alpha}_B+1)}\left(\frac{\gamma_p^{\mathfrak{B}}}{\gamma_p^f}\right)^P,$$
$$b=\frac{12g_3^{\,2}\rho_{\mathfrak{B}}^{(1)}}{(\alpha_f^{(1)}-\alpha_{\mathfrak{B}}^{(1)})(\alpha_f^{(1)}-2\bar{\alpha}_B+1)},\quad c=1. \tag{A4}$$

Using Eqs. (A3)–(A4) and assuming $(\gamma_p^{\mathfrak{B}}/\gamma_p^f)^P=10$, as suggested by data,[22] we fit $\langle n_{\bar{p}}\rangle$ data[11] near $s\sim100$ GeV^2 to obtain[24] g_2 and μ given by Eq. (25). We have checked that these values of g_2, μ are not sensitive to $(\gamma_p^{\mathfrak{B}}/\gamma_p^f)^P$ ratio. Thus taking the ratio to be 1 we find $g_2=0.079$ and $\mu=0.75$.

The $\langle n_{\bar{p}}\rangle$ calculations for broken SU(3) models can be done in an analogous way as above. The results for models A and B of Sec. IV are as follows.

Model A: $\langle n_{\bar{p}}\rangle$ for this model also is given by Eq. (A3), but with the following substitutions:

$$a=\frac{2\rho_{\mathfrak{B}}^{(1)}g_2g_3(\gamma_p^{\mathfrak{B}}/\gamma_p^f)^Pe^{-\mu}}{(\alpha_f^{(1)}-\alpha_{\mathfrak{B}}^{(1)})(\alpha_f^{(1)}-2\bar{\alpha}_B+1)}(6e^{\mu\alpha_\rho}+3\sqrt{2}\tan\theta_f^{(1)}e^{\mu\alpha_\phi}),$$
$$b=\frac{4\rho_{\mathfrak{B}}^{(1)}g_3^{\,2}(2\cos^2\theta_f^{(1)}+\sqrt{2}\sin2\theta_f^{(1)}e^{\mu(\alpha_\phi-\alpha_\rho)}+\sin^2\theta_f^{(1)}e^{2\mu(\alpha_\phi-\alpha_\rho)})}{(\alpha_f^{(1)}-\alpha_{\mathfrak{B}}^{(1)})(\alpha_f^{(1)}-2\bar{\alpha}_B+1)}, \tag{A5}$$
$$c=\tfrac{2}{3}\cos^2\theta_f^{(1)}+\frac{1}{3\sqrt{2}}\sin2\theta_f^{(1)}e^{2\mu(\alpha_{K^*}-\alpha_\rho)}+\tfrac{1}{3}\sin^2\theta_f^{(1)}e^{2\mu(\alpha_\phi-\alpha_\rho)},$$

and

$$\alpha_M=\alpha_\rho.$$

Model B: We have

$$\langle n_{\bar{p}}\rangle=e^{-2\mu\alpha_f^{(1)}}\left[\left(\ln\frac{s}{s_0}-4\mu\right)(c+b)-(1+a)^{-2}(\alpha_f^{(1)}-\alpha_{\mathfrak{B}}^{(1)})^{-1}(b+2ac+4ab+2a^2c+3a^2b)\right],$$

where

$$a=\frac{6k_1(2+\sqrt{2}\tan\theta_f^{(1)})e^{-\mu}}{\alpha_f^{(1)}-\alpha_{\mathfrak{B}}^{(1)}}\left(\frac{\gamma_p^{\mathfrak{B}}}{\gamma_p^f}\right)^P,\quad b=\frac{36k_1^{\,2}(\cos^2\theta_f^{(1)}+\sqrt{2}\sin2\theta_f^{(1)}+1)}{(\alpha_f^{(1)}-\alpha_{\mathfrak{B}}^{(1)})}, \tag{A6}$$
$$c=3(\cos^2\theta_f^{(1)}+\sqrt{2}\sin2\theta_f^{(1)}+1)k_3.$$

APPENDIX B

In this appendix, we obtain a relation between $\sin^2\text{“}\theta_{\omega-\mathfrak{B}}\text{”}$ and the “θ_i”, introduced in Sec. III. Before we do so, we briefly recall how the bound on “$\theta_{\omega-\mathfrak{B}}$” was obtained from data in Ref. 6. The authors of Ref. 6 used the following relations[25]:

$$\frac{\gamma_\Delta^\omega-\gamma_\Delta^\rho}{\gamma_\Delta^\rho}\simeq\sin\text{“}\theta_{\omega-\mathfrak{B}}\text{”}\left(\frac{\gamma_\Delta^{\mathfrak{B}}}{\gamma_\Delta^\omega}\right)^P, \tag{B1}$$

$$\frac{\gamma_K^{\mathfrak{B}}}{\gamma_p^{\mathfrak{B}}}=-\sin\text{“}\theta_{\omega-\mathfrak{B}}\text{”}\frac{\gamma_K^\omega}{\gamma_p^{\mathfrak{B}}}. \tag{B2}$$

Estimating the left-hand side of each of these equations from data and using the couplings ratios extracted from data, they obtained the following bound by taking the product of the equations above:

$$|\sin^2\text{“}\theta_{\omega-\mathfrak{B}}\text{”}|\lesssim0.067,\ \text{i.e.,}\ |\text{“}\theta_{\omega-\mathfrak{B}}\text{”}|\lesssim15^\circ.$$

We will calculate the left-hand side of these equations in terms of “θ_i” of our model and, by comparing the coefficients of the appropriate ratios of couplings, obtain the desired relation for $\sin^2\text{“}\theta_{\omega-\mathfrak{B}}\text{”}$. Firstly, we note that the $(\rho_i^{(1)},\text{“}\theta_i\text{”})$ define the residue matrix of $P''^{\pm}$ below threshold, as is given, e.g., for $i=\omega$ in Eq. (24). Since from Eq. (25) we know that g_2 is small, we expect $\sin\text{“}\theta_i\text{”}$ to be small. Therefore terms of $O(\sin^2\text{“}\theta_i\text{”})$ are negligible and so the analog of Eq. (24) for $j=\alpha_i$ can also be written in the following manner:

$$\text{res}P_b''|_{j=\alpha_i}=\begin{bmatrix}\rho_i^{(1)} & \sqrt{\rho_i^{(1)}}\sin\text{“}\theta_i\text{”}\\ \sqrt{\rho_i^{(1)}}\sin\text{“}\theta_i\text{”} & \sin^2\text{“}\theta_i\text{”}\end{bmatrix}. \tag{B3}$$

From Eq. (B3), one immediately recognizes that the renormalized coupling of Reggeon i to any channel, say ab, is related to the planar couplings of ω and $\mathfrak{B}$ to ab,

$$\gamma_{ab}^{i} = \sqrt{\rho_i^{(1)}}\,(\gamma_{ab}^{i})^{P} + \sin\!\text{“}\theta_i\text{”}\,(\gamma_{ab}^{j})^{P}\,, \tag{B4}$$

where $i \neq j$ and $i, j = \omega, \mathfrak{B}$.

By choosing appropriate i, a, b in Eq. (B4) one easily obtains the following relations:

$$\frac{\gamma_{\Delta}^{\omega} - \gamma_{\Delta}^{\rho}}{\gamma_{\Delta}^{\omega}} = \left(\sqrt{\rho_{\omega}^{(1)}}\, e^{-\mu(\alpha_{\omega}^{(1)} - \alpha_M)} - 1\right) + \sin\!\text{“}\theta_{\omega}\text{”}\, e^{-\mu(1-\alpha_M)} \left(\frac{\gamma_{\Delta}^{\mathfrak{B}}}{\gamma_{\Delta}^{\omega}}\right)^{P},$$

$$\frac{\gamma_{K}^{\mathfrak{B}}}{\gamma_{p}^{\mathfrak{B}}} = \sin\!\text{“}\theta_{\mathfrak{B}}\text{”}\,\frac{\gamma_{K}^{\omega}}{\gamma_{p}^{\mathfrak{B}}},$$

where we have used the relation $\gamma_{\Delta}^{\rho} = (\gamma_{\Delta}^{\omega})^{P} e^{-\mu(\alpha_M - 1)}$. Comparing the equations above with Eqs. (B1) and (B2), we obtain

$$\sin^2\!\text{“}\theta_{\omega-\mathfrak{B}}\text{”} = -\,(\sin\!\text{“}\theta_{\omega}\text{”})(\sin\!\text{“}\theta_{\mathfrak{B}}\text{”})\, e^{\mu(\alpha_M - 1)}\,. \tag{B5}$$

Substituting in Eq. (B5) the values of $\sin\!\text{“}\theta_{\omega}\text{”}$ and $\sin\!\text{“}\theta_{\mathfrak{B}}\text{”}$, which can be obtained from appropriate residue matrices, we obtain

$$\sin^2\!\text{“}\theta_{\omega-\mathfrak{B}}\text{”} = \frac{8 g_2^{\,2} g_3^{\,2} (\rho_{\omega}^{(1)} \rho_{\mathfrak{B}}^{(1)})^{3/2} \times 27 \times e^{-\mu(\alpha_{\omega}^{(1)} + \alpha_{\mathfrak{B}}^{(1)} - 3\alpha_M + 1)}}{(\alpha_{\omega}^{(1)} - \alpha_{\mathfrak{B}}^{(1)})^2 (\alpha_{\omega}^{(1)} - 2\bar{\alpha}_B + 1)(\alpha_{\mathfrak{B}}^{(1)} - 2\bar{\alpha}_B + 1)}. \tag{B6}$$

It is quite straightforward to carry out similar calculations in the broken-SU(3) models of Sec. IV and obtain the following expressions for $\sin^2\!\text{“}\theta_{\omega-\mathfrak{B}}\text{”}$.

Model A:

$$\sin^2\!\text{“}\theta_{\omega-\mathfrak{B}}\text{”} = \frac{4 g_2^{\,2} g_3^{\,2} (\rho_{\omega}^{(1)} \rho_{\mathfrak{B}}^{(1)})^{3/2} e^{-\mu(\alpha_{\omega}^{(1)} + \alpha_{\mathfrak{B}}^{(1)} - \alpha_{\rho} + 1)}}{(\alpha_{\omega}^{(1)} - \alpha_{\mathfrak{B}}^{(1)})^2} \frac{(6\cos\theta_{\omega}^{(1)} e^{\mu\alpha_{\rho}} + 3\sqrt{2}\sin\theta_{\omega}^{(1)} e^{\mu\alpha_{\phi}})^2 (\cos\theta_{\omega}^{(1)} - \sqrt{2}\sin\theta_{\omega}^{(1)})}{(\alpha_{\omega}^{(1)} - 2\bar{\alpha}_B + 1)(\alpha_{\mathfrak{B}}^{(1)} - 2\bar{\alpha}_B + 1)}. \tag{B7}$$

Model B:

$$\sin^2\!\text{“}\theta_{\omega-\mathfrak{B}}\text{”} = \frac{4 k_1^{\,2} (6\cos\theta_{\omega}^{(1)} + 3\sqrt{2}\sin\theta_{\omega}^{(1)})^2}{(\alpha_{\omega}^{(1)} - \alpha_{\mathfrak{B}}^{(1)})^2} (\cos\theta_{\omega}^{(1)} - \sqrt{2}\sin\theta_{\omega}^{(1)})\, e^{-\mu(\alpha_{\mathfrak{B}}^{(1)} + \alpha_{\omega}^{(1)} - \alpha_{\rho} + 1)}\,. \tag{B8}$$

[1] See, e.g., H. M. Chan and S. T. Tsou, in *Many Degrees of Freedom in Particle Theory*, proceedings of the International Summer Institute of Theoretical Physics, Bielefeld, 1976, edited by H. Satz (Plenum, New York, 1978), p. 83.

[2] G. F. Chew and C. Rosenzweig, Phys. Rev. D 12, 3907 (1975).

[3] H. M. Chan and S. T. Tsou, Nucl. Phys. B118, 413 (1977).

[4] T. H. Hansson, Rutherford Report No. RL-78-105, 1978 (unpublished).

[5] R. V. Gavai, Nucl. Phys. B162, 350 (1980); B168, 549 (1980).

[6] R. V. Gavai and D. P. Roy, Phys. Lett. 82B, 139 (1979).

[7] For the specific cases of Refs. 3 and 4, the estimate of Ref. 6 needs to be pushed up by ~50%. Even then it seems quite low compared to the predictions of Refs. 3 and 4.

[8] J. Kwiecinski and N. Sakai, Nucl. Phys. B106, 44 (1976).

[9] J. W. Dash, S. T. Jones, and E. K. Manesis, Phys. Rev. D 18, 303 (1978).

[10] We will be using θ-function thresholds since they are easy to manipulate and also constitute the popular choice.

[11] M. Antinucci *et al.*, Lett. Nuovo Cimento 6, 121 (1973).

[12] H. M. Chan, J. E. Paton, S. T. Tsou, and S. W. Ng, Nucl. Phys. B92, 13 (1975).

[13] We are assuming here that $A(j)$ and $D(j)$ are of such form that $P'_{\pm}$ has simple poles as its leading singularities. In most of the DTU models it is indeed the case.

[14] S. T. Jones, Phys. Rev. D 19, 2792 (1979).

[15] Since in one-dimensional models there is no difference in crossed and uncrossed loops, contributions of $B^{(1)}$ and $C^{(1)}$ are identical to those of $B^{(2)}$ and $C^{(2)}$, respectively (Ref. 3). This explains a factor of 2 for B and C in Eqs. (21). The remaining numerical factors arise from $\sqrt{3}$'s coming from each quark half loop of the corresponding diagram.

[16] In the s plane all these ρ_i's will get multiplied by $(s_0)^{\alpha_{\text{pla}} - \alpha_{\text{ren}}}$. Thus $\rho_f^{(1)} = 1.03$ for $s_0 = 0.6$ GeV^2, which corresponds to the choice of $\bar{s} = 6$ GeV^2 and $\bar{\varkappa} = 2.3$ of Refs. 12 and 3, respectively.

[17] Since these trajectories are some kind of effective trajectories, it is not necessary that factorization should hold for their residues.

[18] As mentioned in the "Note added" of Ref. 3, the inclusion of the planar diagram of their Fig. 10 ($C^{(2)}$ in our Fig. 1) in the kernel resulted in slightly higher predictions for the intercepts than the accepted phenomenological values. Thus below threshold ($s \leq 100$ GeV^2), $\alpha_f = 1.02$, and $\alpha_{\omega} = 0.56$.

[19] For each ordinary quark half loop a factor of $\sqrt{2}$, and for quark half loops in diquarks a factor of $\sqrt{3}$ has been included in Eq. (34). The origin of the rest of the factors is the same as in the previous section.

[20] S. T. Tsou, Phys. Rev. D 16, 2353 (1977).

[21] P. R. Stevens, G. F. Chew, and C. Rosenzweig, Nucl. Phys. B110, 355 (1975).

[22] R. V. Gavai and D. P. Roy, Nucl. Phys. B137, 301 (1978).

[23] The factor of $\frac{1}{2}$ accounts for the fact that an antibaryon can be an antineutron or an antiproton with equal

probability.

[24]Using the data up to $s = 1000$ GeV^2 for the $\langle n_{\bar{p}} \rangle$ fit in addition to what has already been used, we found that μ remains same but g_2 goes up by ~50%, which also pushes up the sin"$\theta_{\omega\text{-}\mathcal{B}}$" by ~50%. However, we do not favor this fit as it is not good near $s \sim 100$ GeV^2. It may be mentioned here that the fit of Ref. 3, which also presumably used data for $100 < s < 1000$ GeV^2, was similarly not good near $s \sim 100$ GeV^2 and that accounts partly for their overestimation of g_2 (i.e., a factor of 1.5).

[25](cos"$\theta_{\omega\text{-}\mathcal{B}}$" − 1) terms, i.e., terms of $O($"$\theta_{\omega\text{-}\mathcal{B}}$"^{2}) are neglected (Ref. 6) in Eq. (B1).